HHS Public Access

Author manuscript

Ecotoxicol Environ Saf. Author manuscript; available in PMC 2020 April 15.

Published in final edited form as:

Ecotoxicol Environ Saf. 2019 April 15; 170: 77–86. doi:10.1016/j.ecoenv.2018.11.107.

Biocorona formation contributes to silver nanoparticle induced endoplasmic reticulum stress

Indushekhar Persaud[1], **Jonathan H. Shannahan**[2], **Achyut J. Raghavendra**[3,4], **Nasser B. Alsaleh**[1], **Ramakrishna Podila**[3,4], and **Jared M. Brown, Ph.D.**[1,*]

[1]Department of Pharmaceutical Sciences, Skaggs School of Pharmacy and Pharmaceutical Sciences, University of Colorado, Aurora, CO 80045, USA

[2]School of Health Sciences, College of Health and Human Sciences, Purdue University, West Lafayette, IN 47907, USA

[3]Department of Physics and Astronomy, Clemson University, Clemson, SC 29634, USA

[4]Clemson Nanomaterials Center and COMSET, Clemson University, Anderson, SC 29625, USA

Abstract

Prior research has demonstrated cells exposed to silver nanoparticles (AgNPs) undergo endoplasmic reticulum (ER) stress leading to cellular apoptosis and toxicity, however, the fundamental mechanism underlying AgNP-induced ER stress is unknown. We hypothesize the biophysical interactions between AgNPs and adsorbed proteins lead to misfolded proteins to elicit an ER stress response. Our investigation examined rat aortic endothelial cells (RAEC) exposed to 20 or 100 nm AgNPs with or without a biocorona (BC) consisting of bovine serum albumin (BSA), high density lipoprotein (HDL) or fetal bovine serum (FBS) to form a complex BC. The presence of a BC consisting of BSA or FBS proteins significantly reduced uptake of 20 nm and 100 nm AgNPs in RAEC. Western blot analysis indicated robust activation of the IREα and PERK pathways in RAEC exposed to 20 nm despite the reduction in uptake by the presence of a BC. This was not observed for the 100 nm AgNPs. Hyperspectral darkfield microscopy qualitatively confirmed that the preformed BC was maintained following uptake by RAEC. Transmission electron microscopy demonstrated a size dependent effect on the sub-cellular localization of AgNPs. Overall, these results suggest that AgNP size, surface area and BC formation governs the induction of ER stress and alterations in intracellular trafficking.

Keywords

ER stress; AgNP; nanoparticle toxicity; protein corona; Nanotoxicology; hyperspectral imaging

*Corresponding Author, Jared M. Brown Ph.D., Department of Pharmaceutical Sciences, Skaggs School of Pharmacy and Pharmaceutical Sciences, University of Colorado Anschutz Medical Campus, 12850 E Montview Blvd, Aurora, CO 80045, United States of America, 303-724-8213, jared.brown@ucdenver.edu.

Introduction

Engineered nanomaterials (ENMs) are utilized in numerous commercial products and recent advancements have increased their potential applications including uses in nanomedicine [1]. For example, silver nanoparticles (AgNPs) are commonly used in numerous consumer and medical products due to their anti-microbial properties [2]. Increased usage of AgNPs in consumer and biomedical applications will result in increased exposures of the general population to these ENMs. These exposures may occur through inhalation, ingestion, dermal exposure or medical applications such as intravenous lines and catheters, which would lead to direct interaction with the circulatory system [3]. Importantly, it has been demonstrated that AgNPs are cytotoxic, immunotoxic and genotoxic using various *in vitro* and *in vivo* models [4–7].

The ER is an organelle that is responsible for the folding and processing of misfolded proteins. Following mRNA translation, proteins are folded within the ER and transported for cellular function. Misfolded proteins are recognized by cells and are transported back to the ER for degradation or autophagy. However, if this system is overwhelmed with an accumulation of misfolded proteins, cells will then undergo an unfolded protein response (UPR) by the dissociation of BIP, an ER chaperone, from ER membrane proteins PERK, IREα, and ATF6 in the ER. This may result in an increase in the folding capacity of cells, arresting mRNA translation, leading to autophagy and/or the induction of apoptosis [8,9]. While recent studies have shown that AgNPs induce an ER stress response in cells and mice [10,11], the fundamental mechanism of this response to AgNP exposure is yet to be understood. For example, it is not known if AgNPs or other ENMs reach the ER or if ER stress occurs through other mechanisms such as oxidative stress or the UPR. It is also unknown how the addition of specific proteins to the surface of AgNPs may influence these responses.

ENMs entering the circulatory system inadvertently encounter proteins, lipids and other macromolecules present in serum resulting in physi- and chemisorption of protein onto the ENM's surface. This biocorona (BC), which presents a new biological identity to the ENM, is dependent upon the ENM physicochemical properties such as surface charge, size and shape. The interactions between ENM and proteins forming the BC often results in protein denaturing and unfolding [9,12–14]. Others and our studies have demonstrated that BC formation affects the physicochemical properties, toxicity, cellular interactions, biodistribution, and genotoxicity of ENMs [13,15–28]. Shannahan et. al. have shown BSA, HDL, and various other proteins in FBS binding to silver nanoparticles [24]. The ENM-BC is a dynamic entity that constantly exchanges weakly bound biomolecules in the BC for proteins with higher affinity for the ENM surface. Gleaning from our earlier studies, adsorbed proteins in ENM-BC often undergo structural transformations and may eventually exacerbate ER stress through the UPR.

In the current study, we tested the hypothesis that formation of a BC on AgNPs contributes to ER stress responses in rat aortic endothelial cells (RAEC). We utilized three explicitly formed BCs on AgNPs that consisted of bovine serum albumin (BSA), high-density lipoprotein (HDL) and a complex BC comprised of proteins in fetal bovine serum (FBS),

which is based on common proteins nanoparticles will encounter in serum. The rational for the investigation of these specific BCs are based on prior work in our lab, which demonstrated similar proteins associated with various nanoparticles. Briefly, albumin and HDL were commonly associated with all the NPs tested. In addition to testing these specific BC we have included a complex BC formed by FBS, which is a mixture of various proteins. [24]. Further, FBS is used in the majority of cell culture studies in the field and therefore represents a common BC that will form during *in vitro* testing of nanoparticle toxicity. Overall our investigation demonstrated the BC contributes significantly to the induction of ER stress and intracellular trafficking of AgNPs within endothelial cells.

Materials and methods:

Silver nanoparticle characterization and biocorona formation

Citrate capped AgNPs with a diameter of 20 nm or 100 nm were purchased from nanoComposix (San Diego, CA, USA). Sizes of purchased AgNPs were confirmed via transmission electron microscopy (TEM) (Supp. Fig 1). Specifically, TEM demonstrated a diameter of 21.92 +/− 3.03 nm for 20 nm AgNPs and 91.07 +/− 6.54 nm for 100 nm AgNPs. Three BCs were formed on the surface of AgNPs using bovine serum albumin (BSA), high-density lipoprotein (HDL) (Sigma Aldrich, St. Louis, MO, USA) or fetal bovine serum (FBS) (Corning, Manassas, VA, USA) to form a complex BC consisting of multiple proteins. Guidelines for forming the BC were based on previous studies [13,24]. Briefly AgNPs were incubated in phosphate buffered saline (PBS) containing BSA or HDL at a concentration of 350 μg/ml overnight at 4°C on a rotisserie mixer. For the complex BC the AgNPs were incubated with a 10% FBS solution in PBS overnight at 4°C on a rotisserie mixer. The AgNPs were pelleted by centrifugation at 20,000g for 10 minutes. The supernatant was aspirated and resuspended in water to a final AgNP concentration of 1mg/ml. Hydrodynamic diameter and zeta potential were measured using dynamic light scattering on a Malvern Zetasizer Nano ZS particle sizer (Worcestershire, UK). Measurements for the hydrodynamic diameter were conducted in deionized (DI) water or unsupplemented DMEM/F12 medium at a concentration of 20 μg/ml (n=3/group). Zeta potential was measured in water at a concentration of 10 μg/ml for AgNPs which was an optimal concentration allowing measurement of zeta potential. Surface area was calculated using the following equation:

$$SA = N \times sa \quad 1)$$

$$sa = 4\pi r^2 \quad 1.1.$$

Equation (1) was used to calculate the total surface area by multiplying total number of AgNPs (N) by apparent surface area (*sa*) of each individual particle. Equation (1.1) was used to calculate surface area (*sa*) of each individual particle by multiplying $4 \times \pi \times \text{radius}^2$[29]. All measurements were made with or without addition of BCs.

Impact of the biocorona on nanoparticle dissolution was measured by inductively coupled mass spectrometry (ICP-MS). Nanoparticles with and without a biocorona were incubated in unsupplemented DMEM/F12 at 37 °C for 24 hrs. The solution was than centrifuged at 10,000g for 10min to pellet nanoparticles. The supernatant was than measured for dissolved Ag ions in the media (n=3).

Circular Dichroism Spectroscopy

Room temperature Circular Dichroism (CD) spectra were measured using a Jasco Spectropolarimeter (J-810, Jasco, Tokyo, Japan). All measurements were carried out in a quartz cell with 10 mm path length with a scanning speed of 50 nm/min in 190–280 nm wavelength range. The results are represented in terms of mean residue ellipticity (theta) in deg cm^2 $dmol^{-1}$. CAPITO (a CD Analysis & Plotting Tool) was used to estimate secondary structure content viz. alpha helices, beta sheets and irregular structures in both pure and adsorbed BSA (n=3) [30]. As described in the preceding section. AgNPs were incubated in 350 ug/ml BSA overnight for biocorona formation. Subsequently, AgNP-BSA suspension was centrifuged at 20,000g for 10 mins and the supernatant was resuspended in water at 1 mg/ml AgNP concentration for performing CD studies. We did not perform CD studies on complex biocorona in FBS due to the presence of a wide range of proteins, which prohibits estimation of secondary structure similar to BSA.

Cell culture and viability studies

Rat aortic endothelial cells (RAEC) and media were purchased from Cell Applications Inc. (San Diego, CA, USA). Cells were cultured at 5% CO_2 and 37°C in cell culture flask and assays were performed at 80% confluency. To prevent the addition of proteins to the pre-established BC, all studies were conducted in unsupplemented media (DMEM/F12). RAEC were seeded in 96-well plates, after 48hrs washed with PBS and the media was replaced with unsupplemented DMEM/F12. Cells were exposed to AgNPs with or without BCs (BSA, HDL, or FBS) at concentrations of 5, 10, 15, 20 and 25 μg/ml for 3hrs or 24hrs. A CellTiter 96® Aqueous One Solution Proliferation Assay (Thermo Fisher Scientific) was conducted to measure viability. The plates were read at 490 nm on a Biotek Synergy HT microplate reader (Winooski, VT, USA) and percent cell viability was calculated comparing exposed cells to untreated control cells. Studies were performed with biological (n=3) and technical replicated (n=3).

Measurement of cell association of silver nanoparticles

RAECs were cultured as previously described and exposed to AgNPs with or without various BCs (BSA, FBS, and HDL). Cells were exposed to AgNPs with or without a BC, in 6 well plates,for 3hrs to measure RAEC association of AgNPs. After 3hrs of exposure to AgNPs the cells were washed with PBS and trypsinized with 250 μL 0.25% trypsin for 5 min at 37°C. Following incubation, trypsin was neutralized with supplemented media and the cells were pelleted. Media was removed and the pellet was washed three times with PBS. An inductively coupled plasma mass spectrometer (ICP-MS, X series II, Thermo Scientific) was used to quantify presence of Ag^+ in cell pellets. Samples (n=3/group) were dissolved in 6ml of 2% nitric acid and measured by ICP-MS using Li, Y and In as an internal standard with a limit of detection of 6 ppb (n=3) [25].

Assessment of endoplasmic reticulum stress

RAECs were grown to 80% confluency in 100mm petri culture plates, washed three times with PBS and unsupplemented DMEM/F12 media was added to each plate. Cells were exposed to 20 nm or 100 nm AgNPs (20μg/ml) with or without a BC (BSA, FBS, or HDL). After a 3hr incubation, cells were washed with cold PBS, scraped to avoid any protease membrane reaction from exposure to trypsin, and pelleted by centrifugation [31]. The cells were resuspended in lysis buffer (1% SDS, 80mM Tris HCL, protease inhibitor cocktail and phosphatase inhibitor cocktail (Sigma-Aldrich, St. Louis, MO, USA)). Proteins were separated using 12% Tris-glycine gels (ThermoFisher Scientific, Waltham, MA, USA) and transferred to nitrocellulose (GE Healthcare Life Sciences; Marlborough, MA, USA) using an X Cell II blot module (Thermo Fisher Scientific, Waltman, MA, USA). Western blots were probed using antibodies against phosphorylated-PERK (pPERK), PERK, CHOP and IRE (Cell Signaling Technology, Danvers, MA, USA); phosphorylated-IRE (pIRE), ATF6 (Abcam, Cambridge, MA, USA); and actin (Sigma Aldrich, St Louis, MO, USA). Secondary antibodies (goat anti-mouse, goat anti-rabbit) were purchased from Li-Cor Biosciences and protein expression was imaged on an Odyssey Infrared Imaging System (Lincoln, NE, USA). Densiometric analysis was performed using ImageJ software (National Institute of Health) and all samples were normalized based on actin expression (n=3/group; n=3 biological replicates). Lastly, densiometric analysis was performed and expressed as the amount of protein per μg Ag^+ uptake as determined by ICP-MS described previously.

Oxidative stress measurements

RAECs were grown in 12-well culture plates to 80% confluence and were washed with PBS. The media was changed to unsupplemented media to prevent the addition of proteins to the established BC. Cells were exposed to AgNPs with a particle size of 20 nm or 100 nm with and without a BC (20 μg/ml) for 30 min. Additional RAEC cells were pre-treated with the anti-oxidant N-Acetylcysteine (NAC) at a concentration of 1μM for 24hrs. After pretreatment, the media was changed and cells were exposed to 20 nm or 100 nm AgNPs. The cells were pelleted and washed with PBS three times before adding H2DCFDA (Molecular Probes, Eugene, OR, USA) to measure reactive oxygen species generation. Samples were measured on an Accuri C6 Flow cytometer (BD Biosciences, San Jose, CA, USA) and the mean fluorescence was measured for 10,000 cells (n=3 technical and biological replicates).

Hyperspectral darkfield analysis of internalized silver nanoparticles

RAECs were grown to 80% confluency on chamber slides, washed with PBS and the media was changed to unsupplemented DMEM/F12. Cells were exposed to AgNPs (20 μg/ml) with and without a BC (BSA, HDL, FBS) at a particle concentration of 20 μg/ml for 3hrs. DAPI was added to each well to label the nucleus and the cells were fixed with 4% paraformaldehyde. Samples were imaged on a Cytoviva microscope with a dark field condenser and images were recorded with a hyperspectral camera (Cytoviva®, Auburn, AL, USA). As per the method described by Shannahan et al. each image was recorded at the focal plane of the nucleus as indicated via DAPI staining of the nucleus [25]. This allowed a qualitative assessment of the uptake of AgNPs with or without a BC. A minimum of 1,000

pixels identified visually as internalized AgNPs were chosen for hyperspectral analysis. Using Envi (ver 4.8) software the selected pixels were used to generate a mean spectral profile, which was then normalized based on intensity. In a separate evaluation AgNPs with or without BCs were loaded onto a microscope slide and evaluated via hyperspectral darkfield micrsoscopy to determine the mean spectral profiles of extracellular AgNPs and alterations in the spectral profile due to addition of BCs. The mean spectral profiles of extracellular AgNPs were then compared to mean spectral profile of internalized AgNPs for comparison, similar to our previous work (n=3 biological and technical replicates) [25].

Bovine serum albumin (BSA) was labeled with an Alexa Fluor® 488SDP (sulfodicholorphenol) ester (ThermoFisher Scientific, Grand Island, NY, USA). Labeled BSA at a concentration of 10mg/ml was added to a Sephadex® G-25 column to remove any excess fluorescent marker not attached to the protein. The labeled protein was incubated with 20 nm AgNPs to form a fluorescent BC as previously described in our current study. RAECs were cultured in chamber slides to 80% confluency and washed with PBS before adding unsupplemented DMEM/F12. The cells were then exposed to AgNP (20 μg/ml) with or without a fluorescently labeled BSA BC for 1hr. The nucleus was labeled with DAPI and the cells were fixed with 4% paraformaldehyde. Cells were imaged with a Cytoviva® microscope and all images were focused on the plane of the nucleus. The images were assessed for co-localization of AgNPs and the fluorescently tagged BSA to determine if the original BC was maintained following internalization (n=3 biological and technical replicates).

Transmission Electron Microscopy

RAECs were grown on a sapphire disk and were exposed to 20 nm AgNPs (20 μg/ml) for 3hrs. After incubation, the cells were frozen using a Wohlwen Compact 02 high pressure freezer. The cryoprotectant used during the freezing process consisted of 150mM mannitol and 2% sucrose. The cells were then then fixed with 0.25% glutaraldehyde, 0.1% uranylacetate/acetone and were embedded in Lowicryl HM20 resin. The samples were sectioned using a Leica Ultracut UCT. Sections were exposed to anti-PDI, to label the endoplasmic reticulum and gold nanoparticles conjugated with a mouse secondary antibody (Abcam, Cambridge, MA, USA). RAEC were analyzed to determine size-dependent differences in the subcellular localization of 20 nm and 100 nm AgNPs after a 3hr incubation (n=3).

Statistical Analysis

Sample size for quantitative analysis used n=3 for each group. Numerical results were analyzed using a one-way ANOVA with a Tukey's multiple comparison post hoc analysis to determine statistical difference using a p value less than 0.05. All data were analyzed with Graphpad PRISM® (Version 5.01). Data are presented as mean +/− standard error of means.

Results

Silver nanoparticle characterization

AgNPs with or without a BC consisting of bovine serum albumin, HDL or FBS were characterized by measuring hydrodynamic diameter in water and DMEM/F12 while zeta potential was measured in water (Table 1). The ionic strength of DMEM/F12 did not allow accurate measurement of zeta potential and therefore zeta potential was only assessed in DI water for AgNPs with and without BCs. The 20 nm AgNPs without a BC had a hydrodynamic diameter of 37.38 nm as measured in water. We observed a significant increase in hydrodynamic diameter with formation of either a BSA (68.15 nm) or FBS (88.27 nm) BC in contrast, HDL did not significantly alter the hydrodynamic diameter of the 20 nm AgNPs (Table 1). The 100 nm AgNPs without a BC (H_2O suspension) were measured at 122.70 nm and the addition of a BC did not result in notable increases in hydrodynamic diameter, except for particles with a FBS corona (Table 1). The zeta potential of the 20 nm AgNPs was −41 mV and following addition of the BC the charge was reduced (Table 1). All zeta potential values for 20 nm AgNPs remained negative even in the presence of a biocorona signifying colloidal stability. The 100 nm AgNPs with and without a BC also had negative values for the zeta potential. In addition, hydrodynamic diameter was measured in unsupplemented DMEM/F12 since this media was used for the biological assays. The 20 nm AgNPs without a BC had a hydrodynamic diameter of 118.87 nm in unsupplemented DMEM/F12, however nanoparticles with a BSA or FBS BC had a significant size reduction to 73.97 nm and 73.01 nm respectively. Examining the 100 nm AgNPs there was a significant increase in hydrodynamic diameter for particles with a FBS BC compared to 100 nm AgNPs without a BC. Lastly, calculated surface area is also provided in Table 1 for comparison across biological responses. The surface area in general was reduced as the BC was formed except for the HDL coated 20 nm AgNPs in which we observed a decrease in hydrodynamic diameter and thus an increase in surface area (Table 1).

The presence of a biocorona did not significantly impact the dissolution of the 20 nm AgNP for the BSA, FBS, or HDL biocorona (1.95, 3.075, 1.91 ppb respectively). A significant increase in dissolution was observed for 20nm for 3hrs and 100 nm at 24hrs AgNPs with a FBS biocorona. For 20 and 100 nm AgNPs with a BSA and HDL biocorona dissolution was not significantly changed (Supp. Figure 2A,B).

Proteins unfold upon the formation of a biocorona on silver nanoparticles

During BC formation, proteins initially adsorb to AgNPs while largely retaining their native-state structure. Subsequently, the adsorbed protein may relax its secondary structure, unfold, and spread out on the AgNP surface depending upon the strength of protein-surface interactions relative to the internal stability of the protein. The adsorption-induced structural changes in BSA were ascertained using CD spectroscopy. As shown in Figure 1A, the CD spectra showed clear evidence for conformational changes of BSA upon BC formation on both 20 and 100 nm AgNPs. The secondary structure of BSA (particularly, the peak relating to α-helical content) significantly disappeared upon its adsorption onto AgNPs and may be explained in terms of soft nature or low internal stability of BSA. Furthermore, the maximum helical content reduction was observed on 20 nm AgNP likely due to higher

curvature. It is expected that the observed changes in the protein structure will increase ER stress, as evidenced by our data discussed in the following sections. Unlike BSA, the secondary structure of proteins in FBS cannot be conclusively assessed due to its heterogeneity.

Silver nanoparticles have minimal effect on cell viability at low doses and early time points

RAEC viability was determined by MTS assay following exposure to AgNPs at concentrations of 5, 10, 15, 20, and 25 μg/ml at 3hrs and 24hrs with or without a BC (Figure 1B and Supp. Figure 3). We observed no significant reduction in viability of RAEC after 3hrs of exposure to AgNPs with or without a BC. However, we did observe a significant reduction in viability in cells exposed to 20 nm AgNPs with or without a BC after 24h (Supp. Figure 3). A reduction in viability was not observed in RAEC exposed to 100 nm AgNPs with or without a BC at either time point (Figure 1B and Supp. Figure 3). All subsequent experiments were performed at time points of 3 hrs or less to limit cytotoxicity.

Biocorona formation decreases association of silver nanoparticles with rat aortic endothelial cells

RAECs were exposed to 20 nm or 100 nm AgNPs with or without a BSA, FBS, or HDL BC for 3 hrs and the amount of cellular uptake was measured using ICP-MS (Figure 1C). 20 nm AgNPs without a BC had the highest uptake concentration of Ag^+ in RAEC (148 ppb). The addition of all three BCs resulted in a significant decrease in uptake. Similarly, a reduction in uptake by the addition of the BSA and FBS BCs were also observed for 100 nm AgNPs. There was no significant decrease in uptake of AgNPs by RAEC for 100 nm AgNPs with a HDL BC.

Biocorona formation influences silver nanoparticle directed ER stress responses in rat aortic endothelial cells

To investigate the influence of a BC on AgNP directed ER stress responses, we examined the three key pathways of ER stress induction including PERK, IREα, and ATF6. RAEC exposure to 20 nm AgNPs with or without a BC activated the IREα and PERK pathways, while the ATF6 pathway was not significantly affected (Figure 2A-E). This activation included increased phosphorylated IREα (pIREα) and phosphorylated PERK (pPERK) levels in RAEC exposed to 20 nm AgNPs with or without a BC (Figures 2A, B, E). In addition to activation of the IREα and PERK pathways by 20 nm AgNPs, we also observed downstream activation of both phosphorylated JNK (pJNK) and CHOP (Figures 2A, C, E). The addition of a BC on the 20 nm AgNPs did not significantly alter the pIREα/IREα or pPERK/PERK ratios when normalized to the actin loading controls (Figure 2E). Similarly, the 100 nm AgNPs preferentially activated the IREα and PERK pathways while having no effect on the ATF6 pathway of ER stress (Figure 2A, B, E). In general, the induction of ER stress pathways by 100 nm AgNPs was significantly less than that observed with the 20 nm AgNPs. Specifically, the formation of a BC on the 100 nm AgNPs had minimal effect on activation of the IREα and PERK pathways when compared to the actin loading control. Lastly, there was no significant difference observed for BIP and XBP1 in RAECs exposed to AgNPs (20 and 100 nm) with or without a BC (Figure 2D and E).

Since we observed a significant reduction in cellular uptake of 20 nm AgNPs with the addition of a BC (BSA, HDL or FBS) as compared to AgNPs without a BC, we plotted the expression of ER stress proteins per μg of AgNP uptake (Figure 3A-D). Taking into consideration the dosimetry of AgNPs, we observed a significant increase in pIRE/IRE ratios for 20 nm AgNPs with a BSA and HDL BC compared to uncoated AgNPs. Similarly, we observed a significant increase in pPERK/PERK in cells exposed to 20 nm AgNPs with a BSA, FBS, or HDL BC compared to uncoated AgNPs (Figure 3C). Calculating pJNK per AgNP uptake levels indicated a significant increase in expression in RAEC exposed to AgNP with a BSA BC (Figure 3B) while CHOP was increased in RAEC exposed to 20 nm AgNP with a BSA and FBS BC. However, no significant change in pIRE/IRE or pJNK levels were observed for RAEC exposed to 100 nm AgNPs with and without a BC when dosimetry was considered.

Oxidative stress does not significantly contribute to the early ER stress response following silver nanoparticle exposure in rat aortic endothelial cells

Oxidative stress is reported to play a role in cellular ER stress responses, therefore we examined RAECs exposed to AgNPs for increases in reactive oxygen species (ROS) [32]. Measuring the conversion of H_2DCFDA to 2',7'-dichlorofluorescein (DCF) indicated there was no significant increase in ROS in RAECs following AgNP exposure (Figure 3E). In fact, we observed no significant change in the basal level of ROS in RAEC following exposure to both 20 and 100 nm AgNPs for 30min (Figure 3E). Further, RAEC treated with N-acetylcysteine (NAC) reduced the basal level of ROS, and treatment with AgNPs did not further increase ROS (Figure 3F). To further confirm that ROS was not playing a role in ER stress responses following RAEC exposure to AgNPs, we measured pIREα/IREα and CHOP levels in cells pre-treated with NAC and exposed to 20 nm or 100 nm AgNPs. Pretreatment of RAECs with NAC did not affect IRE, pIREα or CHOP levels in RAEC exposed to 20 or 100 nm AgNPs suggesting that ROS does not play a significant role in the ER stress response observed (Figure 3F).

The biocorona is carried into rat aortic endothelial cells and silver nanoparticles do not reach the endoplasmic reticulum

Darkfield images confirm 20 nm AgNPs with or without a BC are internalized by RAEC and a reduction in uptake occurs due to the addition of the BCs, qualitatively confirming the ICP-MS data (Figure 4A). To evaluate changes in the BC following cellular uptake, hyperspectral analysis was performed on the 20 nm AgNPs internalized in RAEC. The hyperspectral profiles of AgNPs with or without BCs was compared between non-internalized and internalized particles to investigate any changes in spectral profile which may indicate changes in the BC composition (Figure 4B & S3) [25]. The hyperspectral profile of the 20 nm AgNPs without a BC indicated a red shift and broadening of the peak after cellular internalization when compared to non-internalized AgNPs. This is likely indicative of the association of cellular macromolecules on the surface of 20 nm AgNPs during internalization. 20 nm AgNPs with a BSA or FBS BC displayed a similar hyperspectral profile both inside and outside of the cell suggesting minimal changes in BC composition upon cellular uptake. 20 nm AgNPs with a HDL BC however demonstrated a blue-shift in the hyperspectral profile following internalization by RAECs, possibly due to a

loss of HDL proteins during or following uptake (Figure 4B). An overlay of the three AgNPs with a BC indicated a similar spectral profile following internalization suggesting an intracellular normalization of the BC (Supp. Figure 4).

To further determine if the BC is carried into the cell by AgNPs, RAEC were exposed to 20 nm AgNPs with a fluorescently tagged BSA BC. Using a combination of fluorescent and darkfield microscopy, we observed cellular uptake of AgNPs, but more importantly we observed intracellular co-localization of fluorescently tagged BSA with the AgNPs in RAECs (Figure 5A–D). This demonstrates that the fluorescently tagged BSA remained associated with the AgNPs intracellularly (Figure 5D). We next determined the subcellular localization of AgNPs in RAEC using transmission electron microscopy (TEM). Interestingly, we did not observe either 20 nm or 100 nm AgNPs localized within or near the ER (Figure 5E–H). Further, we found that 20 nm AgNPs were localized within multivesicular bodies (Figure 5E and F), while the 100 nm AgNPs were found within the lysosomal organelle of RAEC (Figure 5G and H) demonstrating different cellular trafficking based upon nanoparticle size.

Discussion

In this study we investigated the role of the BC on AgNP induction of ER stress in rat aortic endothelial cells. Overall, we observed a differential ER stress response between 20 nm and 100 nm AgNPs that primarily consisted of activation of the IREα and PERK pathways. Further, we found that cellular internalization of AgNPs was significantly reduced by the presence of the BC however similar levels of IREα activation were observed suggesting a role for the BC in ER stress.

Similar to prior studies on AgNP cellular effects, our results have demonstrated RAEC exposed to 20 nm AgNPs resulted in the induction of ER stress through activation of the PERK and IREα pathway, which can potentially result in the induction of apoptosis in cells [10,11]. Similar to our findings, Huo et al. showed that mice exposed to AgNPs by pulmonary instillation had an upregulation in pIREα and pPERK levels in lung tissue [10]. Zhang et al. also demonstrated similar results due to exposure to AgNPs in human Chang liver cells [11]. Our results indicate similar trends, while also building upon these previous findings by examining differences in nanoparticle size on the induction of ER stress as well as the influence of the BC. Silver nanoparticles with a size of 20 nm had higher levels of IREα compared 100 nm AgNPs. Prior *in vitro* studies indicate smaller AgNPs ranging from 5–15 nm were more toxic compared to larger particles likely due to increased surface area [33–36]. While there is evidence that AgNPs induce ER stress, the mechanisms involved such as oxidative stress, cellular uptake, trafficking, and a role for the BC has not been reported.

ER stress has a relation to the redox state of cells for protein folding, therefore an acute increase in oxidative stress could lead to the degradation of proteins resulting in the induction of an UPR [37]. ENMs have been shown to induce toxicity through the formation of reactive oxygen species [33,38], however, in our study, oxidative stress was not responsible for AgNP-induced ER stress which was demonstrated by the inability of the

antioxidant N-acetylcysteine to reduce IREα expression following AgNP exposure. Taken together, these findings suggest that AgNP directed ER stress was driven by a mechanism other than oxidative stress.

Since oxidative stress was not playing a major role in AgNP induced ER stress responses, we investigated two additional possibilities for ER stress induction. First, the BC influences cellular uptake of AgNPs leading to ER stress and subsequently, proteins dissociating from AgNPs could be modified and transported to the ER resulting in an unfolded protein response. An alternative mechanism is AgNPs could possibly be transported to the endoplasmic reticulum modifying the protein structure in the organelle resulting in a direct ER stress response.

Interestingly, the formation of a BC affected the intracellular accumulation of AgNPs by reducing uptake of AgNPs in RAEC. Prior studies have indicated the formation of a BC can affect how cells recognize ENMs and reduce cellular adhesion and biological identity, which can affect uptake of ENMs [39–41]. The presence of a BC in our study reduced uptake, however the BC present on AgNPs induced an equivalent ER stress response to uncoated AgNPs as measured by phosphorylation of PERK and IREα. Importantly, when we considered cellular dosimetry and examined ER stress responses in relationship to the amount of AgNPs taken up by RAEC, we revealed a significant role of the BC in activating ER stress pathways. Further, comparison of the 20 nm and 100 nm AgNPs reveals ER stress occurs in RAEC primarily with the 20 nm AgNPs which have a much higher surface area as compared to the 100 nm AgNPs on a mass basis. These findings suggest that both surface area and the BC contribute to ER stress responses in RAEC.

Since there was a decrease in uptake of BC coated AgNPs yet we still observed a significant ER stress response, we investigated whether the BC was maintained and carried into cells possibly contributing to ER stress. Prior research has demonstrated the biocorona is associated with internalized nanoparticles [28,42]. Based on hyperspectral imaging data, a BC consisting of BSA or FBS undergoes minimal changes upon internalization, while we did observe spectral changes in the HDL BC suggesting the possibility that additional proteins are added or replaced within the BC upon cellular uptake. In addition, using BSA as a model protein, we demonstrated that BSA is maintained on AgNPs following internalization suggesting that these ENMs can carry the protein into the cell.

Lastly, to further define this mechanism, we examined subcellular localization to determine whether 20 nm or 100 nm AgNPs reach the ER directly. Our results indicate that 20 nm AgNPs are localized in multivesicular bodies and are not trafficked to the ER. Conversely, the 100 nm AgNPs were found within lysosomes, did not reach the ER, and did not induce an ER stress response. These findings along with our data demonstrating that AgNPs can carry a BC into cells at 1hr and the BC is primarily maintained up to 3 hrs as demonstrated by hyperspectral analysis suggests that the protein constituents of the BC are likely contributing to the ER stress response.

Overall, these findings suggest that the AgNPs do not reach the ER but can carry proteins or gain new protein identity upon cellular internalization. Previous work in our lab and others

has demonstrated that formation of a BC on AgNPs leads to protein structural changes including alterations in the number of α-helices and β-sheets [13]. Moreover Ding et al. demonstrated misfolding of ubiquitin on AgNPs and Podila et al. has shown BSA adsorbed to carbon nanotubes resulted in changes in α-helices demonstrating significant changes in protein structure [18,43]. In addition Wen et al. also demonstrated cytoskeletal protein binding to AgNPs resulted in changes in secondary protein structure [44]. In addition, Ag^+ has been shown to bind to proteins [45], and may stabilize conformational changes in protein structure, which cells may recognize as an unfolded protein. Taken together, based on our current and previous studies, we anticipate that misfolded proteins transported with AgNPs augment an ER stress response compared to pristine AgNPs.

In conclusion, our findings demonstrated a role for BC formation on AgNP induced ER stress possibly through the UPR. Further, we demonstrated a nanoparticle size dependency on subcellular localization and the induction of ER stress. Importantly, while the presence of a BC significantly reduced cellular uptake of AgNPs, ER stress responses remained present at much lower AgNP concentrations suggesting a role for the BC in these adverse responses. Further, the induction of ER stress appears to be through an indirect mechanism as AgNPs do not reach the ER suggesting that proteins in the BC are possibly being released and inducing the UPR (Figure 6). Taken together, these findings suggest that ER stress induced by AgNPs is dependent upon ENM size, surface area and BC formation. Future studies of ENM toxicity should consider the importance of the BC and its effect on cellular dosimetry and stress responses.

Supplementary Material

Refer to Web version on PubMed Central for supplementary material.

Acknowledgements:

We would like to thank Mary Morphew, Courtney Ozzello, Thomas Giddings and Garry Morgan of the University of Colorado Boulder Electron Microscopy Services with their help for TEM imaging.

Funding: This work was funded by the U.S. National Institute of Environmental Health Sciences grants R01 ES01933 and R15 ES022766.

References:

1. Pelgrift RY, Friedman AJ (2013) Nanotechnology as a therapeutic tool to combat microbial resistance. Adv Drug Deliv Rev 65: 1803–1815. [PubMed: 23892192]
2. Prabhu S, Poulose EK (2012) Silver nanoparticles: mechanism of antimicrobial action, synthesis, medical applications, and toxicity effects. International Nano Letters 2: 32.
3. Phalen RF, Morrow PE (1973) Experimental inhalation of metallic silver. Health Phys 24: 509–518. [PubMed: 4707665]
4. AshaRani PV, Low Kah Mun G, Hande MP, Valiyaveettil S (2009) Cytotoxicity and genotoxicity of silver nanoparticles in human cells. ACS Nano 3: 279–290. [PubMed: 19236062]
5. Foldbjerg R, Dang DA, Autrup H (2011) Cytotoxicity and genotoxicity of silver nanoparticles in the human lung cancer cell line, A549. Arch Toxicol 85: 743–750. [PubMed: 20428844]
6. Jiang X, Miclaus T, Wang L, Foldbjerg R, Sutherland DS, et al. (2015) Fast intracellular dissolution and persistent cellular uptake of silver nanoparticles in CHO-K1 cells: implication for cytotoxicity. Nanotoxicology 9: 181–189. [PubMed: 24738617]

7. Vandebriel RJ, Tonk EC, de la Fonteyne-Blankestijn LJ, Gremmer ER, Verharen HW, et al. (2014) Immunotoxicity of silver nanoparticles in an intravenous 28-day repeated-dose toxicity study in rats. Part Fibre Toxicol 11: 21. [PubMed: 24885556]
8. Schroder M, Kaufman RJ (2005) ER stress and the unfolded protein response. Mutat Res 569: 29–63. [PubMed: 15603751]
9. Mehta SB, Bee JS, Randolph TW, Carpenter JF (2014) Partial Unfolding of a Monoclonal Antibody: Role of a Single Domain in Driving Protein Aggregation. Biochemistry 53: 3367–3377. [PubMed: 24804773]
10. Huo L, Chen R, Zhao L, Shi X, Bai R, et al. (2015) Silver nanoparticles activate endoplasmic reticulum stress signaling pathway in cell and mouse models: The role in toxicity evaluation. Biomaterials 61: 307–315. [PubMed: 26024651]
11. Zhang R, Piao MJ, Kim KC, Kim AD, Choi JY, et al. (2012) Endoplasmic reticulum stress signaling is involved in silver nanoparticles-induced apoptosis. Int J Biochem Cell Biol 44: 224–232. [PubMed: 22064246]
12. Gagner JE, Lopez MD, Dordick JS, Siegel RW (2011) Effect of gold nanoparticle morphology on adsorbed protein structure and function. Biomaterials 32: 7241–7252. [PubMed: 21705074]
13. Shannahan JH, Podila R, Aldossari AA, Emerson H, Powell BA, et al. (2015) Formation of a protein corona on silver nanoparticles mediates cellular toxicity via scavenger receptors. Toxicol Sci 143: 136–146. [PubMed: 25326241]
14. Podila R, Chen R, Ke PC, Brown JM, Rao AM (2012) Effects of surface functional groups on the formation of nanoparticle-protein corona. Appl Phys Lett 101: 263701. [PubMed: 23341687]
15. Ban DK, Paul S (2016) Protein corona over silver nanoparticles triggers conformational change of proteins and drop in bactericidal potential of nanoparticles: Polyethylene glycol capping as preventive strategy. Colloids Surf B Biointerfaces 146: 577–584. [PubMed: 27424088]
16. Chen R, Choudhary P, Schurr RN, Bhattacharya P, Brown JM, et al. (2012) Interaction of lipid vesicle with silver nanoparticle-serum albumin protein corona. Appl Phys Lett 100: 13703–137034. [PubMed: 22271932]
17. Chen R, Radic S, Choudhary P, Ledwell KG, Huang G, et al. (2012) Formation and cell translocation of carbon nanotube-fibrinogen protein corona. Appl Phys Lett 101: 133702. [PubMed: 23093808]
18. Ding F, Radic S, Chen R, Chen P, Geitner NK, et al. (2013) Direct observation of a single nanoparticle-ubiquitin corona formation. Nanoscale 5: 9162–9169. [PubMed: 23921560]
19. Gebauer JS, Malissek M, Simon S, Knauer SK, Maskos M, et al. (2012) Impact of the nanoparticle-protein corona on colloidal stability and protein structure. Langmuir 28: 9673–9679. [PubMed: 22524519]
20. Lundqvist M, Stigler J, Elia G, Lynch I, Cedervall T, et al. (2008) Nanoparticle size and surface properties determine the protein corona with possible implications for biological impacts. Proc Natl Acad Sci U S A 105: 14265–14270. [PubMed: 18809927]
21. Monopoli MP, Walczyk D, Campbell A, Elia G, Lynch I, et al. (2011) Physical-chemical aspects of protein corona: relevance to in vitro and in vivo biological impacts of nanoparticles. J Am Chem Soc 133: 2525–2534. [PubMed: 21288025]
22. Sasidharan A, Riviere JE, Monteiro-Riviere NA (2015) Gold and silver nanoparticle interactions with human proteins: impact and implications in biocorona formation. Journal of Materials Chemistry B 3: 2075–2082.
23. Shannahan JH, Brown JM, Chen R, Ke PC, Lai X, et al. (2013) Comparison of nanotube-protein corona composition in cell culture media. Small 9: 2171–2181. [PubMed: 23322550]
24. Shannahan JH, Lai X, Ke PC, Podila R, Brown JM, et al. (2013) Silver nanoparticle protein corona composition in cell culture media. PLoS One 8: e74001. [PubMed: 24040142]
25. Shannahan JH, Podila R, Brown JM (2015) A hyperspectral and toxicological analysis of protein corona impact on silver nanoparticle properties, intracellular modifications, and macrophage activation. Int J Nanomedicine 10: 6509–6521. [PubMed: 26508856]
26. Tenzer S, Docter D, Kuharev J, Musyanovych A, Fetz V, et al. (2013) Rapid formation of plasma protein corona critically affects nanoparticle pathophysiology. Nat Nanotechnol 8: 772–781. [PubMed: 24056901]

27. Treuel L, Brandholt S, Maffre P, Wiegele S, Shang L, et al. (2014) Impact of protein modification on the protein corona on nanoparticles and nanoparticle-cell interactions. ACS Nano 8: 503–513. [PubMed: 24377255]
28. Wang FJ, Yu L, Monopoli MP, Sandin P, Mahon E, et al. (2013) The biomolecular corona is retained during nanoparticle uptake and protects the cells from the damage induced by cationic nanoparticles until degraded in the lysosomes. Nanomedicine-Nanotechnology Biology and Medicine 9: 1159–1168.
29. Ho M, Wu KY, Chein HM, Chen LC, Cheng TJ (2011) Pulmonary toxicity of inhaled nanoscale and fine zinc oxide particles: mass and surface area as an exposure metric. Inhal Toxicol 23: 947–956. [PubMed: 22122307]
30. Wiedemann C, Bellstedt P, Gorlach M (2013) CAPITO--a web server-based analysis and plotting tool for circular dichroism data. Bioinformatics 29: 1750–1757. [PubMed: 23681122]
31. Batista U, Garvas M, Nemec M, Schara M, Veranic P, et al. (2010) Effects of different detachment procedures on viability, nitroxide reduction kinetics and plasma membrane heterogeneity of V-79 cells. Cell Biol Int 34: 663–668. [PubMed: 20337597]
32. Malhotra JD, Kaufman RJ (2007) The endoplasmic reticulum and the unfolded protein response. Semin Cell Dev Biol 18: 716–731. [PubMed: 18023214]
33. Carlson C, Hussain SM, Schrand AM, Braydich-Stolle LK, Hess KL, et al. (2008) Unique cellular interaction of silver nanoparticles: size-dependent generation of reactive oxygen species. J Phys Chem B 112: 13608–13619. [PubMed: 18831567]
34. Gliga AR, Skoglund S, Wallinder IO, Fadeel B, Karlsson HL (2014) Size-dependent cytotoxicity of silver nanoparticles in human lung cells: the role of cellular uptake, agglomeration and Ag release. Part Fibre Toxicol 11: 11. [PubMed: 24529161]
35. Liu W, Wu Y, Wang C, Li HC, Wang T, et al. (2010) Impact of silver nanoparticles on human cells: effect of particle size. Nanotoxicology 4: 319–330. [PubMed: 20795913]
36. Mehta SB, Carpenter JF, Randolph TW (2016) Colloidal Instability Fosters Agglomeration of Subvisible Particles Created by Rupture of Gels of a Monoclonal Antibody Formed at Silicone Oil-Water Interfaces. Journal of Pharmaceutical Sciences 105: 2338–2348. [PubMed: 27422087]
37. Malhotra JD, Kaufman RJ (2007) Endoplasmic reticulum stress and oxidative stress: a vicious cycle or a double-edged sword? Antioxid Redox Signal 9: 2277–2293. [PubMed: 17979528]
38. Kim S, Choi JE, Choi J, Chung KH, Park K, et al. (2009) Oxidative stress-dependent toxicity of silver nanoparticles in human hepatoma cells. Toxicol In Vitro 23: 1076–1084. [PubMed: 19508889]
39. Lesniak A, Fenaroli F, Monopoli MP, Aberg C, Dawson KA, et al. (2012) Effects of the presence or absence of a protein corona on silica nanoparticle uptake and impact on cells. ACS Nano 6: 5845–5857. [PubMed: 22721453]
40. Lesniak A, Salvati A, Santos-Martinez MJ, Radomski MW, Dawson KA, et al. (2013) Nanoparticle adhesion to the cell membrane and its effect on nanoparticle uptake efficiency. J Am Chem Soc 135: 1438–1444. [PubMed: 23301582]
41. Yan Y, Gause KT, Kamphuis MM, Ang CS, O'Brien-Simpson NM, et al. (2013) Differential roles of the protein corona in the cellular uptake of nanoporous polymer particles by monocyte and macrophage cell lines. ACS Nano 7: 10960–10970. [PubMed: 24256422]
42. Bertoli F, Garry D, Monopoli MP, Salvati A, Dawson KA (2016) The Intracellular Destiny of the Protein Corona: A Study on its Cellular Internalization and Evolution. ACS Nano 10: 10471–10479. [PubMed: 27797479]
43. Podila R, Vedantam P, Ke PC, Brown JM, Rao AM (2012) Evidences For Charge Transfer-Induced Conformational Changes In Carbon Nanostructure-Protein Corona. J Phys Chem C Nanomater Interfaces 116: 22098–22103. [PubMed: 23243478]
44. Wen Y, Geitner NK, Chen R, Ding F, Chen P, et al. (2013) Binding of cytoskeletal proteins with silver nanoparticles. RSC Advances 3: 22002–22007.
45. Kittler S, Greulich C, Gebauer JS, Diendorf J, Treuel L, et al. (2010) The influence of proteins on the dispersability and cell-biological activity of silver nanoparticles. Journal of Materials Chemistry 20: 512–518.

Highlights

- Silver nanoparticle biocorona formation contributes to endoplasmic reticulum stress
- Biocorona formation significantly affects cellular dosimetry of silver nanoparticles
- Nanoparticle size influences subcellular localization contributing to toxicity
- Biocorona formation should be considered in silver nanoparticle toxicity

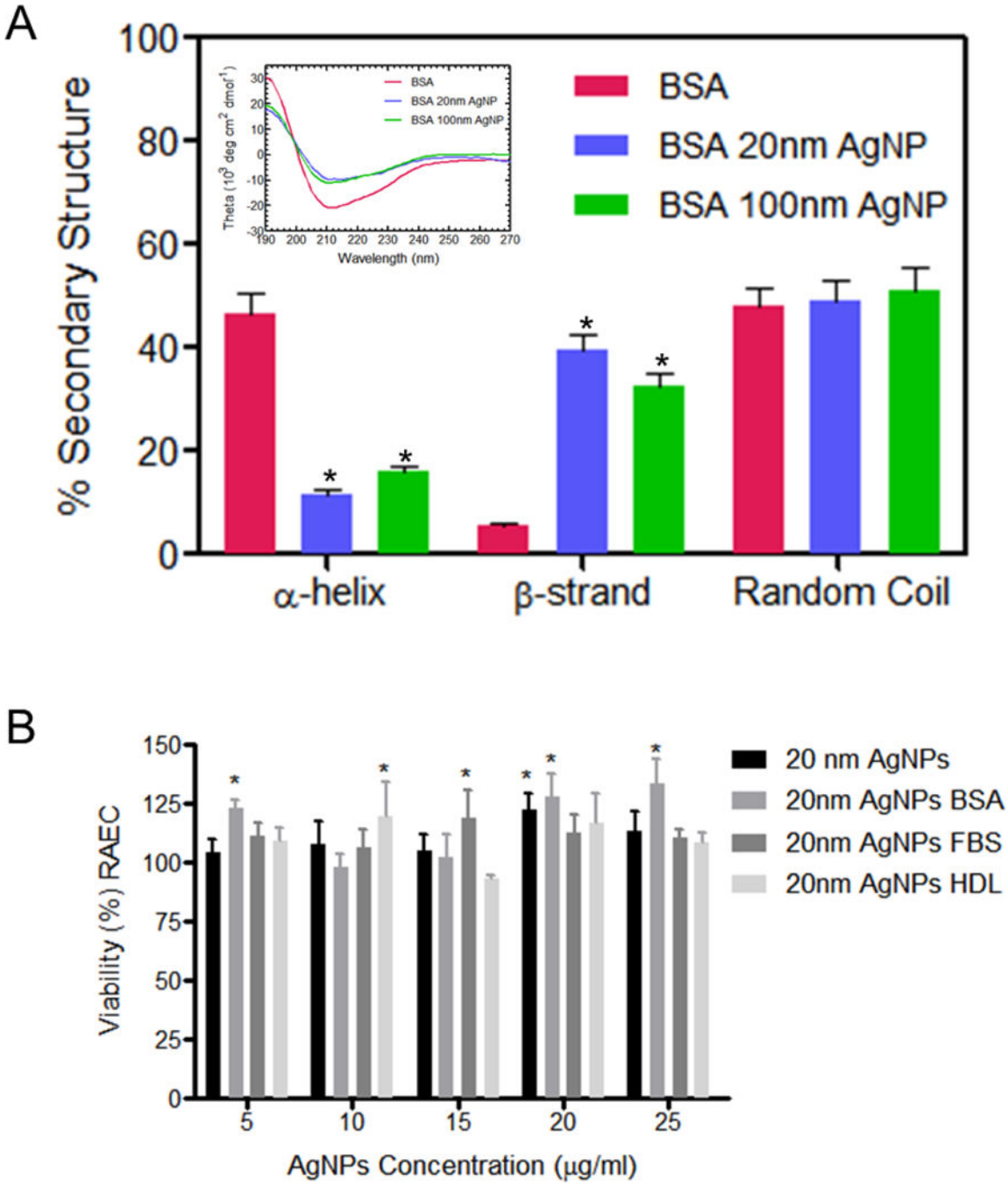

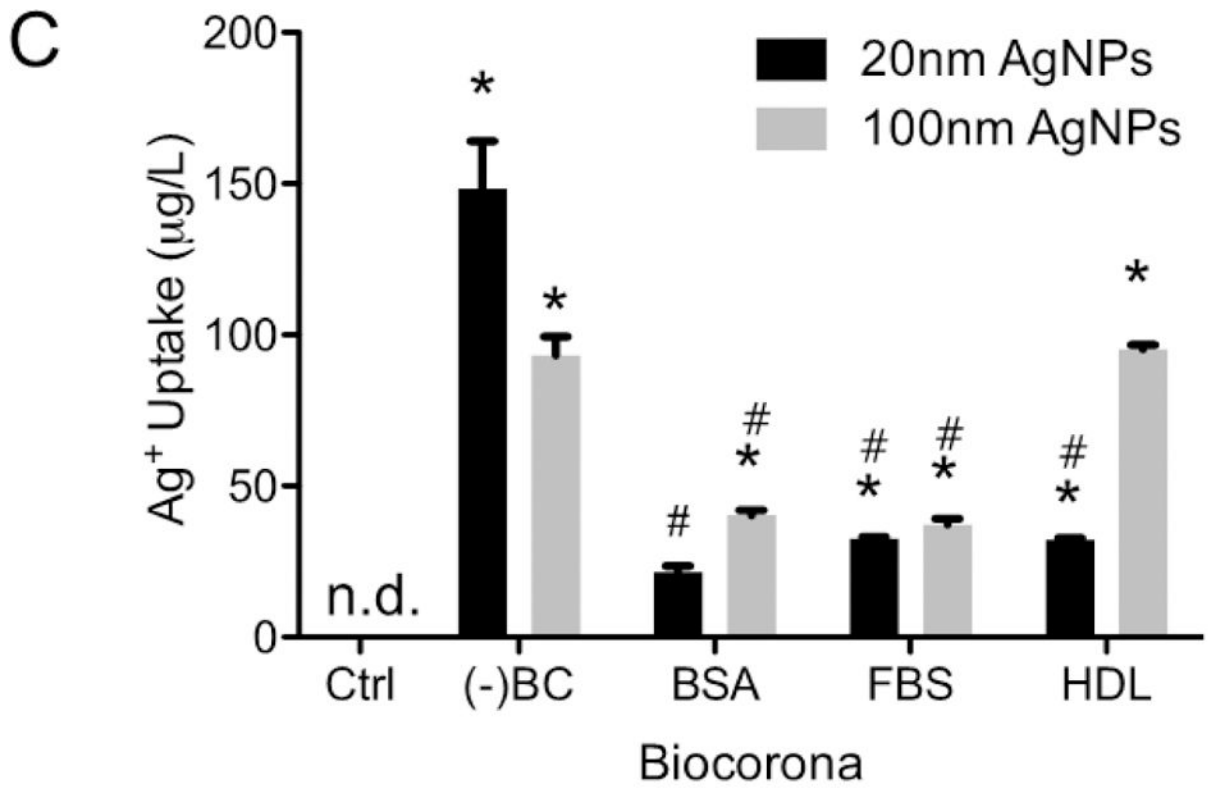

Figure 1: CD spectroscopy of BSA biocorona formed on AgNPs, viability and uptake in RAEC: (A) Circular dichroism (CD) spectra for pure BSA and BSA incubated with 20 and 100 nm AgNPs showed significant decrease in a-helix content with corresponding increase in beta sheets and irregular secondary structure content. The raw spectra are shown in the inset. *-statistically significant compared to BSA protein, $p<0.05$, N=3. (B) Viability as measured by MTS assay of RAEC exposed to 20 nm AgNPs with or without a BC for 3hrs. (C) RAEC were exposed to AgNPs (20 µg/ml) with or without a BC (BSA, HDL or FBS) for 3hrs to measure cell uptake. AgNP uptake was quantified using ICP-MS. (A)*- viability statistically significant compared control group (B) n.d. – not detected, *-statistically significant compared to control, # -statistical significance compared to AgNPs without a biocorona, $p<0.05$ (N=3).

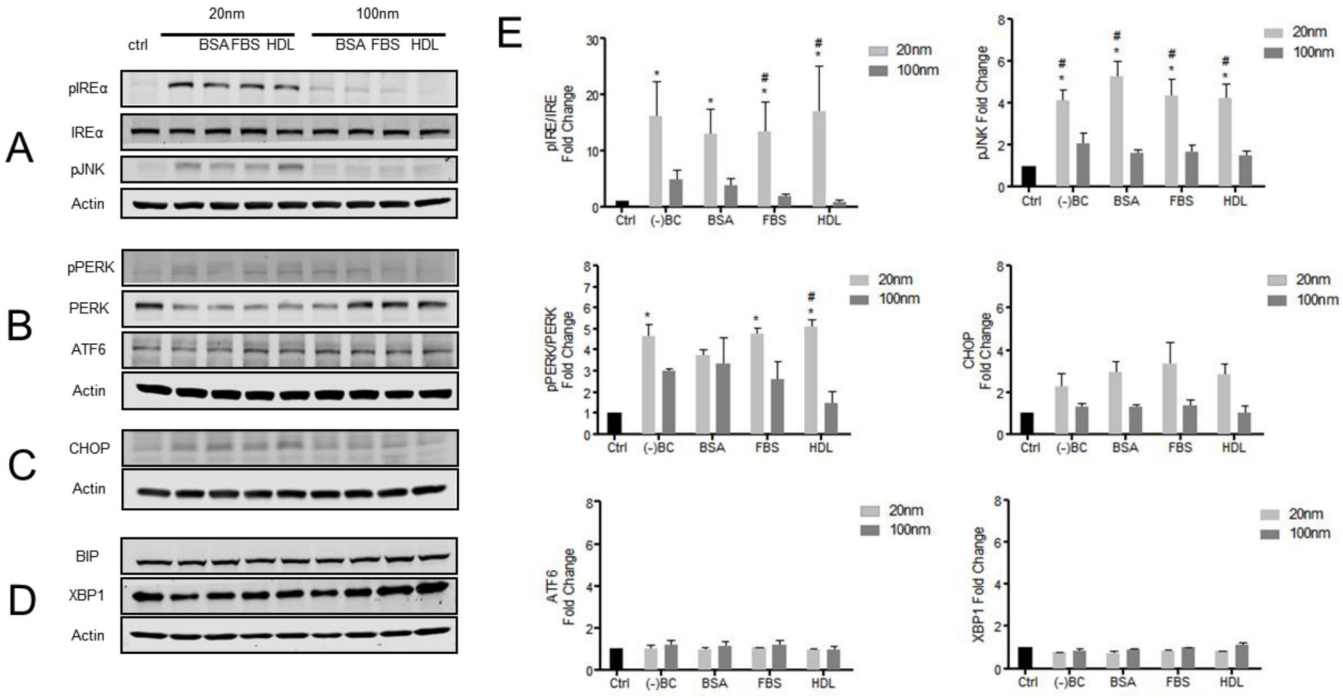

Figure 2: Western blot analysis of ER stress related proteins:

RAEC were exposed to AgNPs (20 μg/ml) with or without a BC for 3hrs and protein expression was measured by Western blot analysis. Densiometric analysis was performed using ImageJ comparing 20nm (light gray) and 100nm (dark gray) AgNPs with a BC (BSA-bovine serum albumin, FBS-fetal bovine serum, HDL-high density lipoprotein). (A) Images of pIREα, IREα, pJNK, and actin expression in RAEC exposed to AgNPs with or without a BC. (B) Images of BIP, XBP1, and actin expression. (C) Images of pPERK, PERK, ATF6, and actin expression. (D) Images of CHOP and actin expression. (E) Densiometric analysis of protein expression measured by western blot studies (N=3). *-statistically significant compared to control ($p<0.05$); #-one way ANOVA indicating a statistically significant compared to 20nm and 100nm with similar BCs.

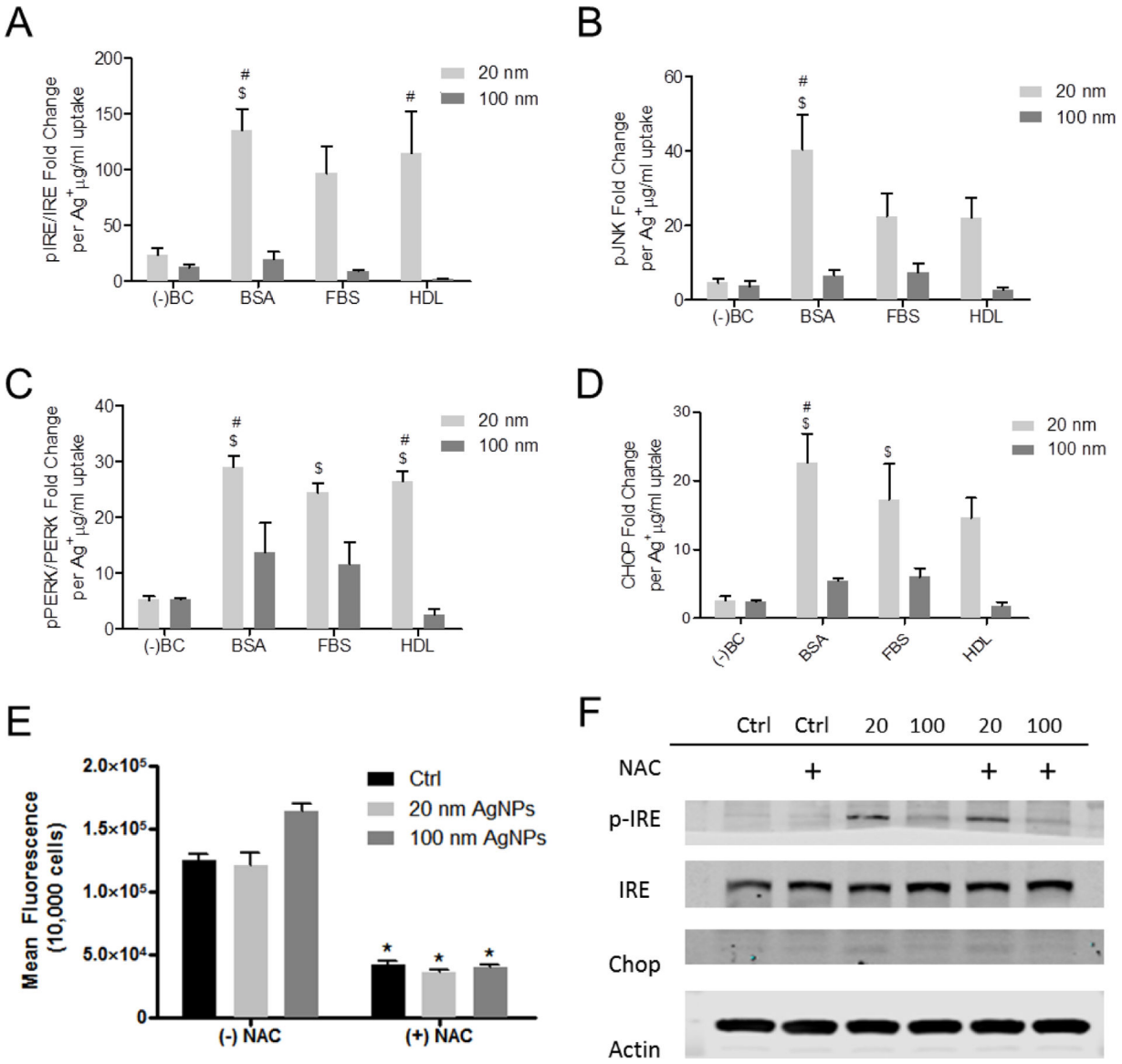

Figure 3: ER stress related protein expression calculated based on AgNP uptake and contribution of reactive oxygen species to silver nanoparticle induced ER stress:

RAEC were exposed to AgNP (20 µg/ml) for 3 hrs. (A) Densiometric analysis of pIRE/IRE per ug/ml of Ag^+ uptake measure by ICP-MS (N=3). (B) Densiometric analysis of pJNK per ug/ml of Ag^+ uptake measure by ICP-MS (N=3). (C) Densiometric analysis of pPERK/ PERK per ug/ml of Ag^+ uptake measure by ICP-MS (N=3). (D) Densiometric analysis of CHOP per ug/ml of Ag^+ uptake measure by ICP-MS (N=3). Reactive oxygen species levels were measured in RAEC by DCF while Western blot analysis was used to investigate the induction of ER stress. (E) Reactive oxygen species measurements in RAEC exposed to 20nm or 100nm AgNPs (20 µg/ml). *statistically significant ($p<0.05$). (F) Images of protein expression measured by Western blot analysis of RAEC pretreated with N-acetylcysteine (NAC) and exposed to 20 nm and 100 nm AgNPs for 3hrs. *statistically significant compared to cells without NAC pretreatment ($p<0.05$).

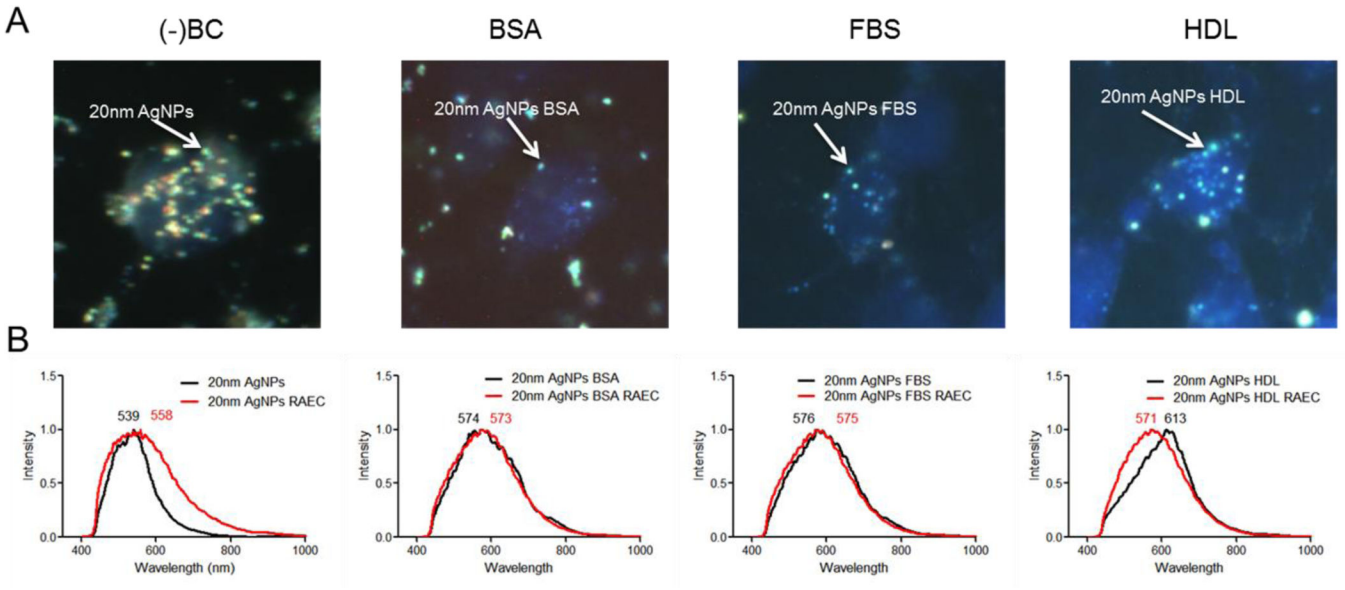

Figure 4: Darkfield and hyperspectral analysis:

(A) Darkfield images were taken of RAEC exposed to 20nm AgNPs (20 μg/ml) with and without a BC. Particles are indicated by bright punctate dots and nucleus in blue (DAPI staining). Images indicate an increase in AgNPs without a BC in RAEC. B) Using hyperspectral analysis, a minimum of 1000 pixels were analyzed for changes in spectral profile of the AgNPs upon internalization. The mean spectral profile of AgNPs (black) were compared to AgNPs internalized in cells (red).

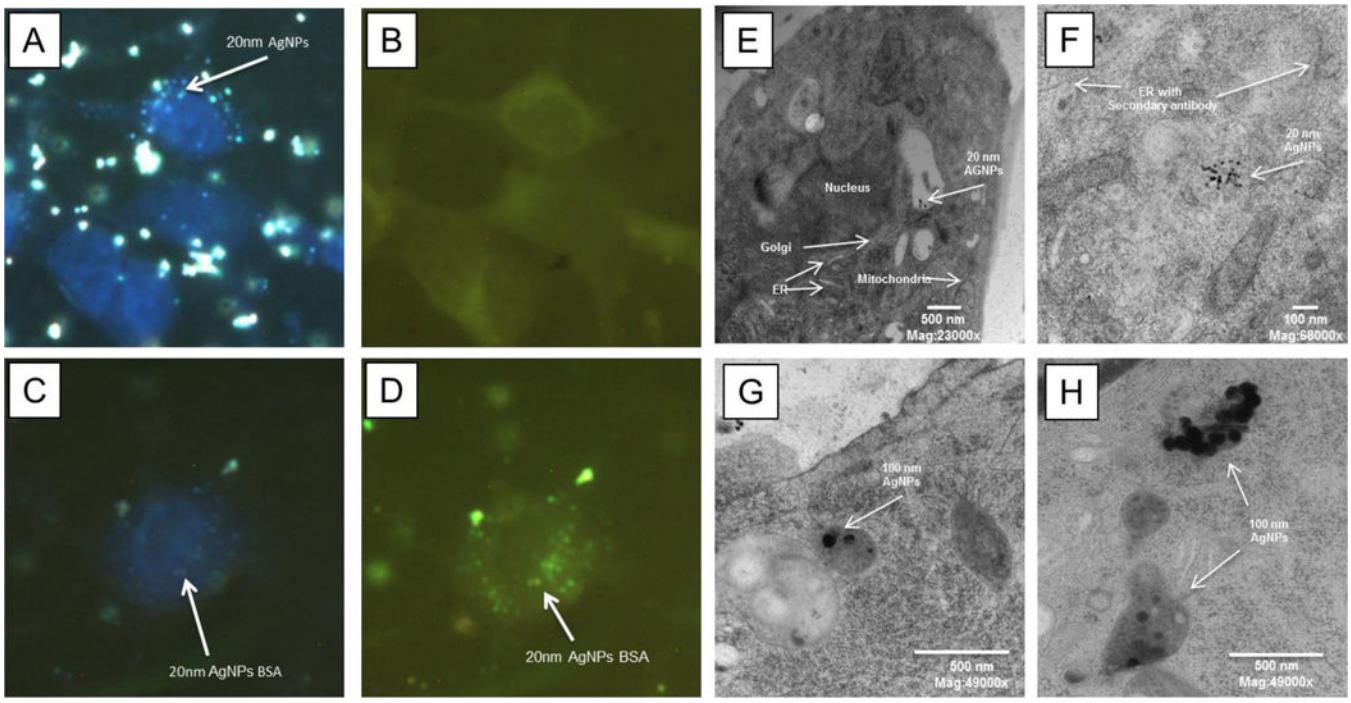

Figure 5: Internalization of AgNPs with a fluorescently tagged biocorona and transmission electron microscopy of RAEC internalized AgNPs:

RAECs were exposed to AgNPs (20 μg/ml) for 1h with a bovine serum albumin BC that was fluorescently tagged. (A) Darkfield images indicate cellular uptake of AgNPs without a biocorona. (B) AgNPs without a fluorescent BSA BC. (C) Darkfield imaging of AgNPs with a fluorescent BSA. (D) Co-localization of AgNPs with a fluorescent BSA BC by darkfield and fluorescent imaging. RAECs were exposed to 20 nm AgNPs for 3 hrs and cells were imaged using TEM. (E,F) 20 nm AgNPs were observed in multi-vesicular bodies. (F) The endoplasmic reticulum was labeled with a PDI antibody followed by a gold secondary antibody. (G,H) The 100 nm AgNPs were observed in lysosomes.

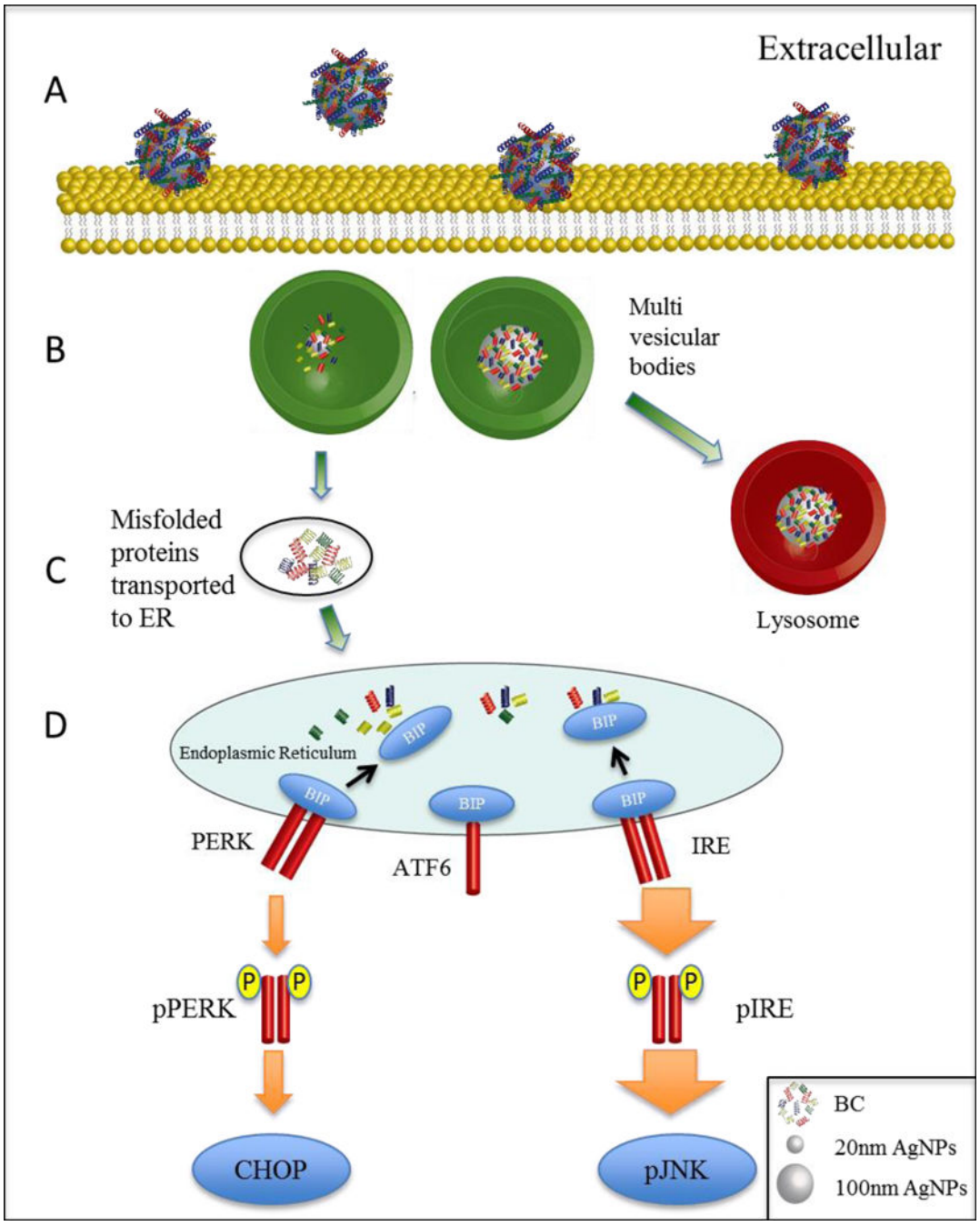

Figure 6: Proposed model for the induction of ER stress by AgNPs.

(A) RAECs are exposed to AgNPs with a BC leading to interaction with the cell membrane. (B) 20 nm AgNPs localize in multivesicular bodies while 100 nm AgNPs are trafficked to the lysosome. (C) The detachment of proteins from AgNP biocorona occurs within the multi-vesicular bodies. (D) Proteins, possibly with a modified structure, are transported to the endoplasmic reticulum resulting in ER stress through the unfolded protein response.

Table 1:

Silver nanoparticle characterization.

Silver nanoparticle hydrodynamic size was measured using dynamic light scattering in DMEM and H_2O. Zeta potential was measured in H_2O for 20nm and 100nm AgNPs with and without a biocrorona.

	H_2O				DMEM/F12		
AgNPs (+/− BC)	**Hydrodynamic size (d.nm)**	**Zeta potential (mV)**	**PDI**	**Surface Area (m^2/g)**	**Hydrodynamic size (d.nm)**	**Surface Area (m^2/g)**	**PDI**
20 nm	37.4 ± 0.4	−41.0 ± 4.8	0.192±0.037	15.3±0.2	118.87 ± 6.16	15.3±0.2	0.223±0.019
20nm BSA	68.2 ± 2.8 *	−9.6 ±1.1	0.258±0.042	8.4±0.3 *	73.97 ± 3.41 *	7.7±0.4 *	0.206±0.035
20nm FBS	85.8 ±2.1 *	−23.8 ±3.49	0.157±0.002	6.7±0.4 *	73.01 ± 1.24 *	7.8±0.1 *	0.450±0.078
20nm HDL	35.9 ±3.8	−26.7±1.1	0.204±0.052	16.0±1.8 *	275.97 ±62.20	2.2±0.6 *	0.337±0.059
100 nm	122.7 ±1.7	−47.3±3.0	0.077±0.030	4.7±0.1	194.73 ±15.99	4.7±0.1	0.163±0.017
100nm BSA	126.1 ±0.8	−11.0±0.2	0.074±0.006	4.5±0.1	157.70 ± 1.47	3.6±0.1	0.175±0.046
100nm FBS	152.0 ±2.2 #	−17.4±1.3	0.071±0.054	3.8±0.1	175.37 ± 1.62 #	3.3±0.1	0.157±0.029
100nm HDL	124.7 ±1.2	−13.8±0.5	0.061±0.013	4.6±0.1	164.57 ±10.91	3.5±0.2	0.131±0.037

*-statistically significant compared to uncoated 20nm AgNPs.

#-statistically significant compared to uncoated 100nm AgNPs. ($p<0.05$, one-way Anova).